CERES_EBAF-Surface_Ed2.7

Data Quality Summary (June 7, 2013)

Investigation: **CERES**
Data Product: **EBAF-Surface**

Data Set: **Terra (Instruments: CERES-FM1 or CERES-FM2)**
Aqua (Instruments: CERES-FM3 or CERES-FM4)

Data Set Version: **Edition2.7**

Subsetting Tool Availability: http://ceres.larc.nasa.gov

The purpose of this document is to inform users of the accuracy of this data product as determined by the CERES Science Team. The document summarizes key validation results, provides cautions where users might easily misinterpret the data, provides links to further information about the data product, algorithms, and accuracy, and gives information about planned data improvements.

This document provides a high-level quality assessment of the CERES EBAF-Surface data product that contains surface fluxes consistent with the top-of-atmosphere fluxes contained in the CERES Energy Balanced and Filled (EBAF-TOA) data product. As such, this document represents the minimum information needed by scientists for appropriate and successful use of the CERES EBAF-Surface data product. For a more thorough description of the methodology used to produce EBAF-Surface, please see Kato et al. (2013). It is strongly suggested that authors, researchers, and reviewers of research papers re-check this document for the latest status before publication of any scientific papers using this data product.

Changes from EBAF-Surface Ed2.6r
- Because clear-sky shortwave (SW) and longwave (LW) top-of-atmosphere (TOA) fluxes over snow and sea ice have been revised in EBAF-TOA from Ed2.6r to Ed2.7, relatively larger changes occur in clear-sky surface downward and upward SW and LW fluxes than in all-sky fluxes especially over polar regions and Tibet. Changes, however, occur in both all-sky and clear-sky.
- Surface fluxes in Ed2.6r were based upon GEOS-4.1 temperature/humidity data from March 2000 through December 2007 and GEOS-5.2 from January 2008 onwards. This introduced a discontinuity, particularly for downward LW surface flux. In EBAF-Surface Ed2.7, a new temperature/humidity dataset (GEOS 5.4.1) that spans the entire CERES record is used to derive corrections to minimize the discontinuity (see Section 4.8 for

details). In addition, near-surface temperature and humidity inaccuracies in GEOS-4.1 over the tropics in 2000 and 2004 in Ed2.6r were reduced (see also Section 4.8 for details).

- Ed2.6r had a coding bug that resulted in a 1° geolocation error in the output file. An IDL code was provided to correct for the 1° longitude shift for Ed2.6r. The coding error was fixed in EBAF-Surface Ed2.7 so users no longer need to apply the correction.

- An upper bound is set to the surface flux adjustment. The maximum value of the perturbation of surface irradiance by a single variable is no more than 10 times the standard deviation of the distribution of 1°×1° perturbations from that variable over the globe.

- Negative clear-sky net surface SW fluxes are removed. This negative case occurs when the clear-sky SW upward flux is larger than the clear-sky SW downward flux. The negative clear-sky net surface flux occurred in Ed 2.6r when TOA SW is tuned to twilight SW irradiance (Kato and Loeb 2003) over regions where the solar zenith angle is greater than 90°. In Ed2.7, the tuning is not applied to regions where the solar zenith angle is greater than 90°.

*NOTE: To navigate the document, use the Adobe Reader bookmarks view option.
Select "View" "Navigation Panels" "Bookmarks".*

TABLE OF CONTENTS

LIST OF FIGURES

LIST OF FIGURES

<u>Figure</u>   <u>Page</u>

LIST OF FIGURES

Figure   Page

LIST OF TABLES

1.0   Introduction

In order to determine the distribution of surface radiation over the globe, the CERES team relies on radiative transfer model calculations initialized using satellite-based cloud and aerosol retrievals and meteorological and aerosol assimilation data from reanalysis to characterize the atmospheric state. The accuracy and stability in computed top-of-atmosphere (TOA) and surface fluxes thus depend upon the quality of the input cloud and atmospheric data (e.g. Rose et al. 2013). The standard CERES data products (e.g., SYN1deg-Month) use cloud and aerosol properties derived from MODIS radiances, meteorological assimilation data from the Goddard Earth Observing System (GEOS) Versions 4 and 5 models, and aerosol assimilation from the Model for Atmospheric Transport and Chemistry (MATCH; Collins et al. 2001).

In order to minimize the error in surface fluxes due to uncertainties in the input data sources, the EBAF-Surface data product introduces several additional constraints based upon information from other independent data sources, such as CERES TOA fluxes, AIRS-derived temperature/humidity profiles, and CALIPSO/CloudSat-derived vertical profiles of clouds.

This document describes the procedure used to determine EBAF surface fluxes and provides an assessment of the uncertainty of the EBAF-Surface product.

2.0   Description of Data Used for EBAF-Surface Production

Surface fluxes in EBAF-Surface are derived from two CERES data products: (i) CERES SYN1deg-Month Ed3 provides computed surface fluxes to be adjusted and (ii) CERES EBAF-TOA Ed2.7 (Loeb et al. 2009, Loeb et al. 2012) provides the CERES-derived TOA flux constraints by observations.

SYN1deg-Month is a Level 3 product and contains gridded monthly mean computed TOA and surface fluxes along with fluxes at three atmospheric pressure levels (70, 200, and 500 hPa). Surface fluxes in SYN1deg-Month are computed with cloud properties derived from MODIS and geostationary satellites (GEO), where each geostationary satellite instrument is calibrated against MODIS (Doelling et al. 2013). The Ed2 CERES cloud algorithm (Minnis et al. 2011) derives cloud properties (e.g. fraction, optical depth, top height, and particle size) from narrowband radiances measured by MODIS twice daily from March 2000 through August 2002 (Terra only) and four times a day after September 2002 (Terra plus Aqua). The Edition 2 two-channel GEO cloud algorithm (Minnis et al. 1995) provides cloud properties (fraction, top height, and daytime optical depth) every three hours between Terra and Aqua observations. Cloud properties are gridded onto a 1°×1° spatial grid and interpolated to 1 hourly intervals (hour boxes) to fill hour boxes with no retrieved cloud properties. Up to four cloud-top heights (cloud types) are retained for each hour box within a 1°×1° grid box. Cloud properties (cloud top height, optical thickness, particle size, phase etc.) are kept separately for four cloud types.

To treat horizontal variability of optical thickness within a cloud type explicitly, both linear and logarithmic means of the cloud optical thicknesses are computed for each cloud type. The distribution of cloud optical thickness expressed as a gamma distribution is estimated from the linear and logarithmic cloud optical thickness means (Barker 1996; Oreopoulos and Barker 1999; Kato et al. 2005). Once the distribution of cloud optical thickness is estimated for each cloud type, a gamma-weighted two-stream radiative transfer model (Kato et al. 2005) is used to compute the shortwave flux vertical profile for each cloud type. The logarithmic mean optical thickness is used in the longwave flux computation with a modified 2-stream approximation (Toon et al. 1989; Fu et al. 1997). The cloud base height, which largely influences the surface downward longwave flux in midlatitude and polar regions, is estimated by an empirical formula described by Minnis et al. (2011).

Temperature and humidity profiles used in the radiative transfer model calculations are from the Goddard Earth Observing System (GEOS-4 and 5) Data Assimilation System reanalysis (Bloom et al. 2005; Rienecker et al. 2008). GEOS-4 is used from March 2000 through December 2007, and GEOS-5 is used beginning January 2008. The GEOS-4 and 5 temperature and relative humidity profiles have a temporal resolution of 6 hours. Spatially, the profiles are re-gridded to 1°×1° maps. Skin temperatures used in the computations are from GEOS-4 and GEOS-5 at a 3-hourly resolution, the native temporal resolution of GEOS-4 skin temperature, although the GEOS-5 product has a higher 1-hourly native resolution available. Other inputs used in SYN1deg-Month include ozone amount (Yang et al. 2000) and ocean spectral surface albedo from Jin et al. (2004). Broadband land surface albedos are inferred from the clear-sky TOA albedo derived from CERES measurements (Rutan et al. 2009).

Computed TOA fluxes from SYN1deg-Month do not necessarily agree with the CERES-derived TOA fluxes from EBAF-TOA Ed2.7, partly because of the error in inputs used in the computations. Input errors also affect computed surface fluxes. To minimize the error in surface fluxes, we use an objective constrainment algorithm to adjust surface, atmospheric, and cloud properties within their uncertainties in order to ensure that computed TOA fluxes are consistent with the CERES-derived TOA fluxes within their observational error. The steps involved are as follows:

- Determine 1°×1° monthly mean differences between the computed TOA fluxes from SYN1deg-Month and the fluxes from CERES EBAF-TOA.
- Correct the TOA longwave bias error caused by the upper tropospheric relative humidity error in GEOS-4 or GEOS-5 using AIRS (AIRX3STM.005) data as the constraint. We also correct for the bias error of the surface downward longwave flux, which is caused by missing the lower cloud layer of overlapping clouds. This bias correction is based upon computed surface fluxes calculated with CALIPSO and CloudSat-derived vertical cloud profiles (Kato et al. 2011). In addition, the surface downward longwave flux bias error caused by differences in boundary layer temperature and humidity between GEOS-4 and GEOS-5.4.1 (March 2000 to December 2007) and GEOS-5.2 and GEOS-5.4.1 (January 2008 to November 2011) is corrected.
- Use a Lagrange multiplier procedure to determine the perturbation of surface, cloud, and atmospheric properties to match the TOA flux differences, assuming that perturbations applied to the input variables are small relative to their respective monthly mean values. Jacobians that are needed to determine surface, cloud, and atmospheric property perturbations, as well as surface flux adjustments, are computed separately and used in the Lagrange multiplier procedure.
- Compute the surface flux change based on these perturbed surface, cloud, and atmospheric properties. Subsequently, the surface flux changes are added to the 1°×1° monthly mean SYN1deg-Month fluxes.

3.0   Cautions and Helpful Hints

The CERES Science Team notes several CAUTIONS and HELPFUL HINTS regarding the use of CERES_EBAF-Surface_Ed2.7:

- The CERES_EBAF-Surface_Ed2.7 product can be visualized, subsetted, and ordered from: (http://ceres.larc.nasa.gov).
- The CERES team has significantly reduced GEO artifacts in CERES_EBAF-Surface_Ed2.7 as compared to surface fluxes included in SYN1deg-Month for two reasons. The GEO-derived cloud fraction errors are corrected based on the cloud fraction derived from CALIPSO and CloudSat, and computed fluxes at TOA are constrained by CERES EBAF-TOA.
- CERES_EBAF-Surface_Ed2.7 does not contain TOA fluxes. The corresponding TOA fluxes are included in CERES_EBAF-TOA_Ed2.7.
- Clear-sky surface fluxes are consistent with clear-sky TOA fluxes included in CERES-EBAF-TOA_Ed2.7. Therefore, the monthly 1°×1° gridded clear-sky fluxes are clear-sky fraction-weighted fluxes instead of fluxes computed by removing clouds. Computed clear-sky fluxes are also constrained by the CERES-derived clear-sky TOA fluxes that are included in CERES_EBAF-TOA_Ed2.7.
- Global means are determined using zonal geodetic weights. The zonal geodetic weights can be obtained from
  (http://ceres.larc.nasa.gov/science_information.php?page=GeodeticWeights).
- Cloud radiative effects are computed as all-sky flux minus clear-sky flux.
- The net flux is positive when the energy is deposited to the surface, i.e. the net is defined as downward minus upward flux.
- The source of temperature and humidity profiles for surface flux calculations changes from GEOS-4.1 to GEOS-5.2.0 starting in January 2008. The discontinuity in a time series of fluxes averaged over a relatively large scale (e.g. averaged over land or ocean) is mostly mitigated by corrections using GEOS-5.4.1 throughout the Ed2.7 period (see Section 4.8 for details).
- Near-surface temperature and humidity inaccuracies exist in GEOS-4 over the tropics in 2000 and 2004 in Ed2.6r. This problem has been mitigated using the difference between GEOS-4.1 or GEOS-5.2.0 and GEOS-5.4.1 in the tuning process (see Section 4.8 for details).
- There are regions where the surface flux adjustments are large, such as over the Andes, Tibet, and central eastern Africa. As a result, the deseasonalized anomalies over these regions can be noisy.
- The MODIS-derived aerosol optical thickness inputs change from Collection 4 to Collection 5. Collection 4 is used through the end of April 2006, and Collection 5 is used thereafter. As a result, a discontinuity and spurious trend can appear in the time series of regional clear-sky SW downward flux deseasonalized anomalies.

4.0   Accuracy and Validation

In this section, surface flux uncertainty and known problems of surface fluxes included in the CERES_EBAF-Surface_Ed2.7 product are discussed.

4.1   Global Annual Mean Flux Comparison

Table 4-1 shows that the input adjustments discussed in Section 2.0 reduce the computed and CERES-derived global annual mean TOA flux difference from -2.3 W m^{-2} to 0.0 W m^{-2} for longwave and from -1.2 W m^{-2} to -0.1 W m^{-2} for shortwave. (Computed values refer to either those from SYN1deg-Month or EBAF-Surface, while CERES-derived values refer to those from EBAF-TOA.) As a result, the global annual mean surface upward and downward longwave fluxes change by 0.5 W m^{-2} and 3.3 W m^{-2}, respectively. Similarly, the surface upward and downward shortwave fluxes change by 0.8 W m^{-2} and -0.7 W m^{-2}, respectively. These changes are within the uncertainties of the surface fluxes estimated by Kato et al. (2012), shown in Table 4-2. Note that computed TOA fluxes are not included in the EBAF-Surface product. Users who need TOA fluxes should use the EBAF-TOA product.

Table 4-1. Global annual mean fluxes using data from March 2000 through February 2010 (W m^{-2}).

	Flux Component	Ed3A SYN1deg-Month	EBAF-Surface Ed2.6r	EBAF-Surface Ed2.7	EBAF-TOA Ed2.7
TOA	Incoming solar	339.9	339.9	339.9	339.9
	LW (all-sky)	237.3	239.7	239.6	239.6
	SW (all-sky)	98.5	99.6	99.6	99.7
	Net (all-sly)	4.06	0.64	0.69	0.63
	LW (clear-sky)	263.7	265.8	265.7	265.8
	SW (clear-sky)	52.5	52.5	52.6	52.6
	Net (clear-sly)	23.6	21.6	21.6	21.6
Surface	LW down (all-sky)	341.8	343.7	345.1	
	LW up (all-sky)	397.6	398.1	398.1	
	SW down (all-sky)	187.2	186.7	186.5	
	SW up (all-sky)	23.3	24.1	24.1	
	Net (all-sky)	108.1	108.3	109.4	
	LW down (clear-sky)	313.5	314.1	315.8	
	LW up (clear-sky)	396.6	398.3	398.4	
	SW down (clear-sky)	242.4	243.4	244.1	
	SW up (clear-sky)	28.7	29.6	29.7	
	Net (clear-sky)	130.6	129.6	131.8	

Table 4-2. Estimated uncertainties (1σ or k = 1) in the flux computed with satellite-derived cloud and aerosol properties in W m^{-2} (after Kato et al. 2012).

			Estimated uncertainty			
		Mean value	Monthly gridded	Monthly zonal	Monthly global	Annual global
Downward longwave	Ocean+Land	345	14	11	7	7
	Ocean	354	12	10	7	7
	Land	329	17	15	8	7
Upward longwave	Ocean+Land	398	15	8	3	3
	Ocean	402	13	9	5	5
	Land	394	19	15	5	4
Downward shortwave	Ocean+Land	192	11	10	6	5
	Ocean	190	11	10	6	5
	Land	203	12	10	7	5
Upward shortwave	Ocean+Land	23	11	3	3	3
	Ocean	12	11	3	3	3
	Land	53	12	8	6	6

4.2   Regional Mean All-Sky Surface Flux Adjustments

Figure 4-1 shows the difference of TOA SW and LW fluxes between EBAF-TOA Ed2.7 and SYN1deg-Month Ed3A. Although adjustments of TOA fluxes are made by perturbing input variables and not directly adjusting fluxes, the difference shown in Figure 4-1 is approximately equal to the TOA flux adjustments. The top plots are 1°×1° 10-year means, and the bottom plots are RMS differences between SYN1deg-Month (untuned) and EBAF-TOA fluxes computed over 1°×1° grids. Over some regions where the edge of sea ice, low-level clouds, and dust aerosols are present, the SW fluxes are adjusted by a large amount. For longwave, large adjustments occur over the Andes, Tibet, and central eastern Africa. Surface irradiance in these regions might contain a larger error than that indicated in the monthly gridded column of Table 4-2.
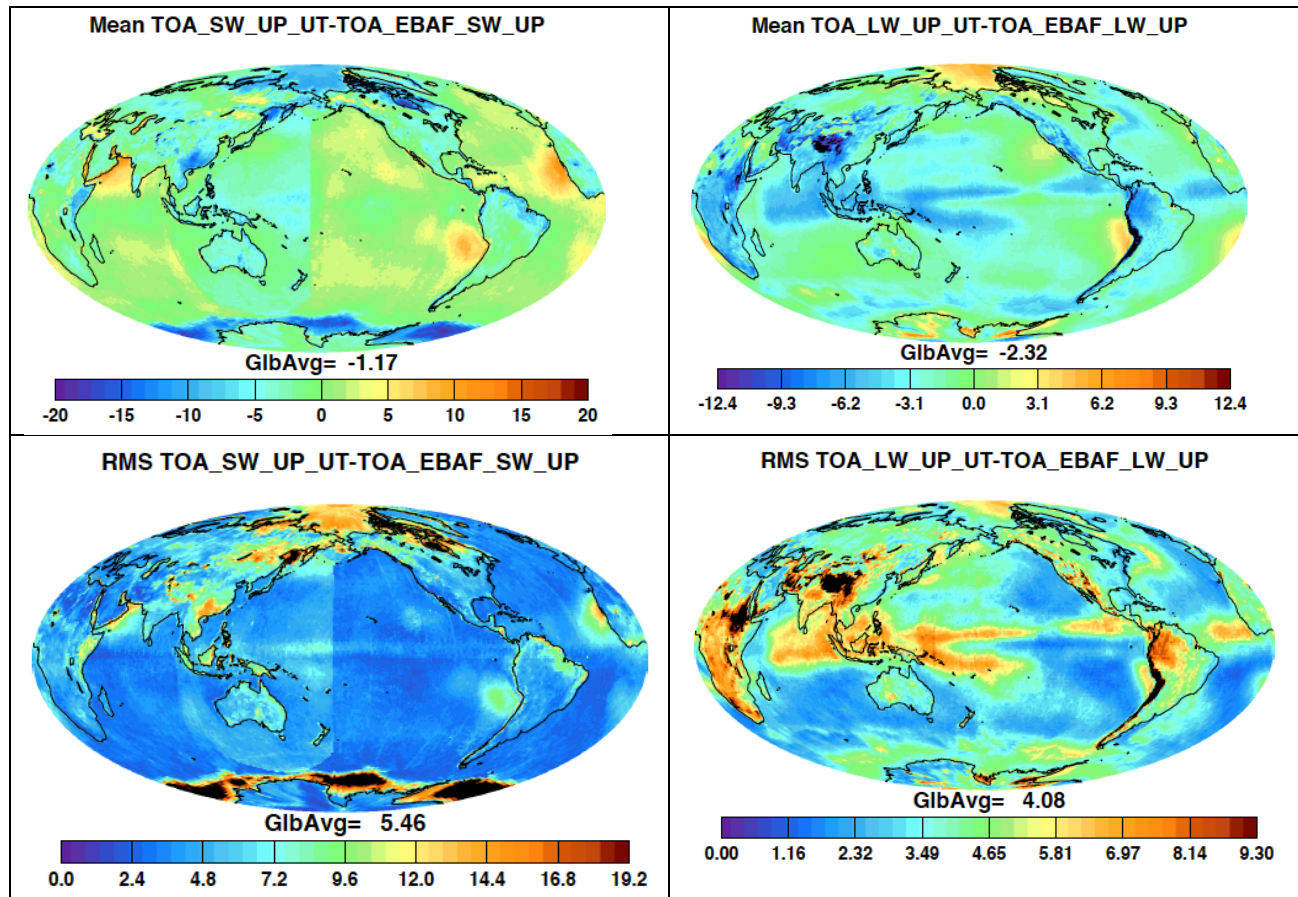
Figure 4-1. (top left) Monthly mean difference and (bottom left) root-mean-square (RMS) difference between SW TOA flux computed in the CERES SYN1deg-Month Ed3A product and observed from CERES EBAF-TOA Ed2.7. The mean and RMS differences are computed using 120 months of data from March 2000 through February 2010. Top right and bottom right plots show the corresponding TOA LW irradiance differences.

Cloud properties derived from geostationary satellites (GEO) are used between 60°N to 60°S to resolve diurnal cycles. Although most GEO artifacts are removed, they are apparent when flux differences are computed, such as atmospheric flux (TOA net minus surface net) or cloud radiative effects (all-sky minus clear-sky fluxes). Figure 4-2 (left) shows an example of an artifact that appears in the net shortwave cloud radiative effect east of Australia. In addition, when the trend of flux is derived from 1°×1° gridded deseasonalized anomalies, artifacts are often apparent (see Figure 4-2 right).
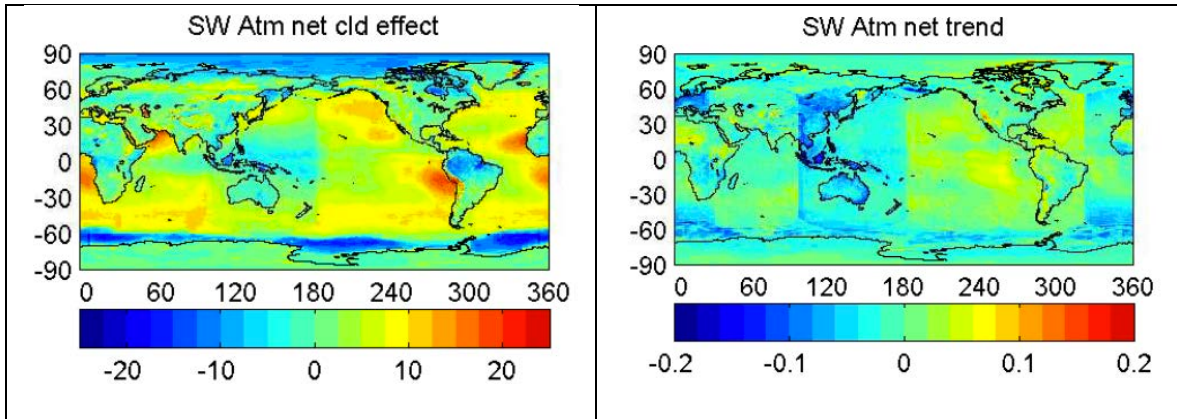
Figure 4-2. (left) Annual mean within-atmosphere absorbed shortwave cloud radiative effect (W m^{-2}) computed from the all-sky minus clear-sky EBAF-TOA–Surface shortwave net flux difference. The cloud effect is computed using 1°×1° gridded 10 years of data. (right) Trend derived from absorbed shortwave flux by the atmosphere. The trend is expressed in W m^{-2} per month.

4.3   Comparison with Surface Observations

Figure 4-3 shows a comparison between monthly 1°×1° gridded fluxes from EBAF-Surface and observed fluxes at 26 surface sites. Table 4-3 summarizes the bias and RMS differences. The RMS differences of monthly mean surface downward shortwave and longwave fluxes are smaller than the uncertainty of monthly gridded fluxes shown in Table 4-2. In addition to land sites, Table 4-3 also shows comparisons over ocean sites. The adjustments applied to the SYN1deg-Month product improve the agreement with surface observations for both SW and LW over oceans and LW over land.
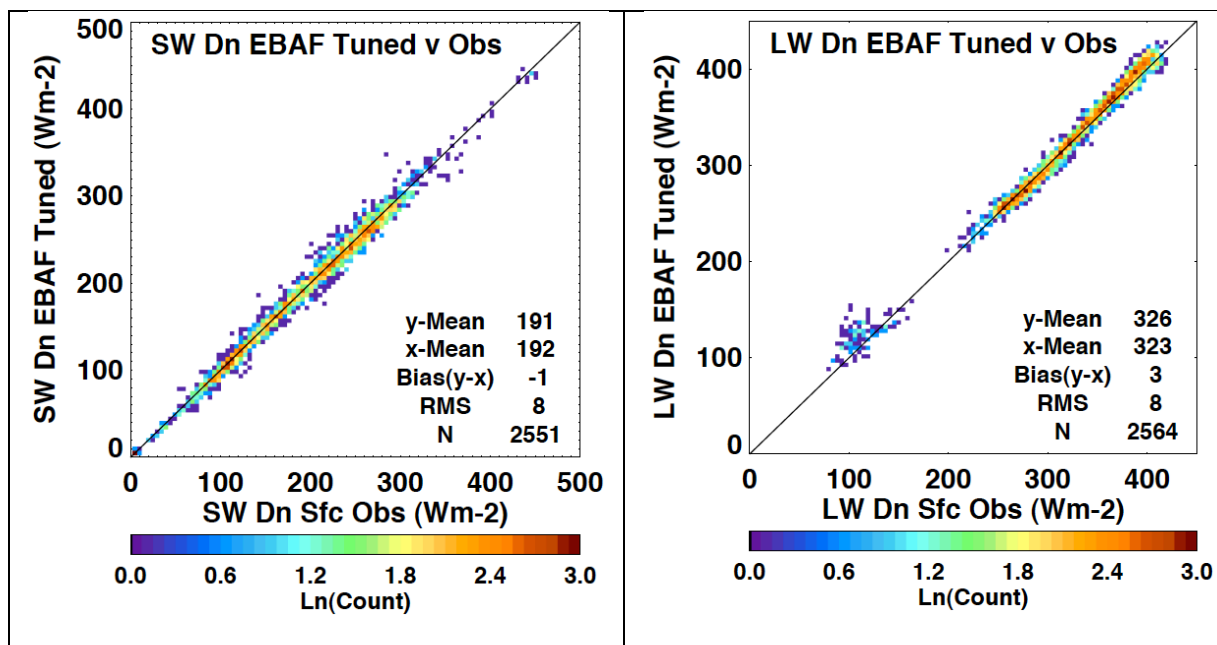
Figure 4-3. Comparison of computed surface flux from EBAF-Surface Ed2.7 with observed fluxes at 26 surface sites for (left) downward shortwave flux and (right) downward longwave flux. Each dot represents a monthly mean value. Twenty-six sites located on relatively uniform terrain are selected. Ten years of data from March 2000 through February 2010 are used.

Table 4-3. Summary of monthly mean bias[1] (and RMS difference) between the two computed products and the observed surface irradiances in W m^{-2} (after Kato et al. 2013).

	Observed mean flux	SYN1deg-Month	EBAF-Surface
Land[2]			
Shortwave down	189.3	0.5 (7.7)	-1.7 (7.9)
Longwave down	317.1	-4.1 (8.5)	2.8 (8.3)
Ocean[3]			
Shortwave down	236.1	4.3 (11.5)	4.9 (12.5)
Longwave down	401.8	-3.5 (5.9)	-2.0 (6.3)

1. Computed minus observed.
2. Observations at 24 sites from March 2000 through February 2010 are used.
3. Available observations at 23 buoys for longwave [4 WHOI buoys, 2 RAMA buoys (McPhaden et al. 2009), 11 TRITON/TAO buoys (McPhaden et al. 1998), 4 PIRATA buoys (Bourlès et al. 2008), and KEO+PAPA from PMEL] and 71 buoys for shortwave (4 WHOI buoys, 17 PIRATA, 14 RAMA, 34 TRITON/TAO, and KEO+PAPA from PMEL) from March 2000 through February 2010 are used.

4.4 Regional Mean Clear-Sky Surface Fluxes

To be consistent with CERES EBAF-TOA and the procedure used for it, the computed 1°×1° gridded monthly mean surface clear-sky fluxes are weighted by the clear-sky fraction determined by imagers. As a result, the monthly gridded mean clear-sky surface flux can be significantly different from the clear-sky flux computed by the method of removing clouds from the column. Figure 4-4, Figure 4-5, and Figure 4-6 show the difference of clear-sky surface and atmospheric fluxes computed using clear-sky fraction weights and those computed by removing clouds. The difference of longwave fluxes is caused by a smaller water vapor amount in clear-sky atmospheres than the amount in all-sky conditions (e.g. Cess and Potter 1987; Sohn et al. 2010). Relatively larger differences of shortwave fluxes predominantly occur over polar regions and are caused by the different sampling of the cryosphere surface; if clear sky predominantly occurs over open ocean versus sea ice, surface shortwave fluxes will be different from those computed by removing clouds.
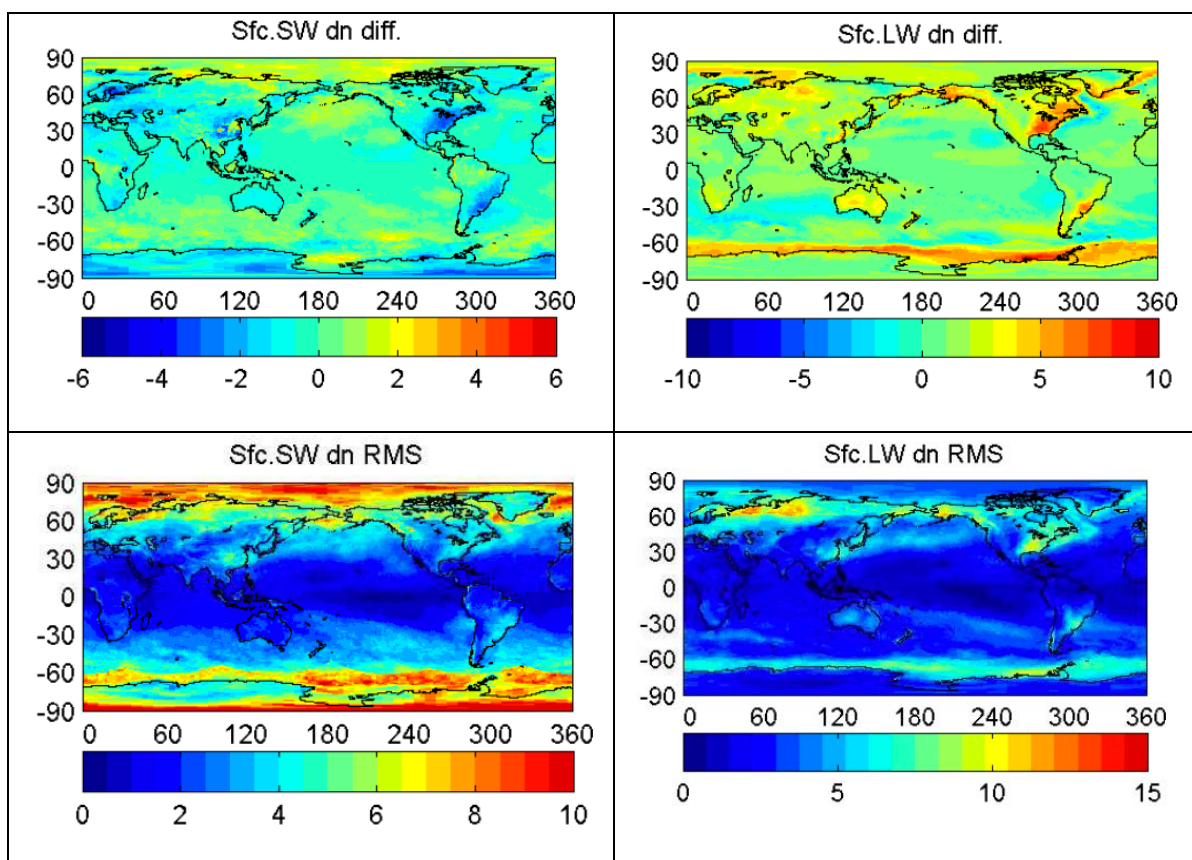
Figure 4-4. (top) Monthly mean difference and (bottom) RMS difference between cloud-removed and clear-sky fraction-weighted (left) surface downward shortwave fluxes and (right) surface downward longwave fluxes in W m^{-2}. The mean difference and RMS difference are computed using 10 years of monthly mean 1°×1° gridded fluxes from March 2000 through February 2010. The mean difference is defined as the clouds-removed minus clear-sky fraction-weighted fluxes.
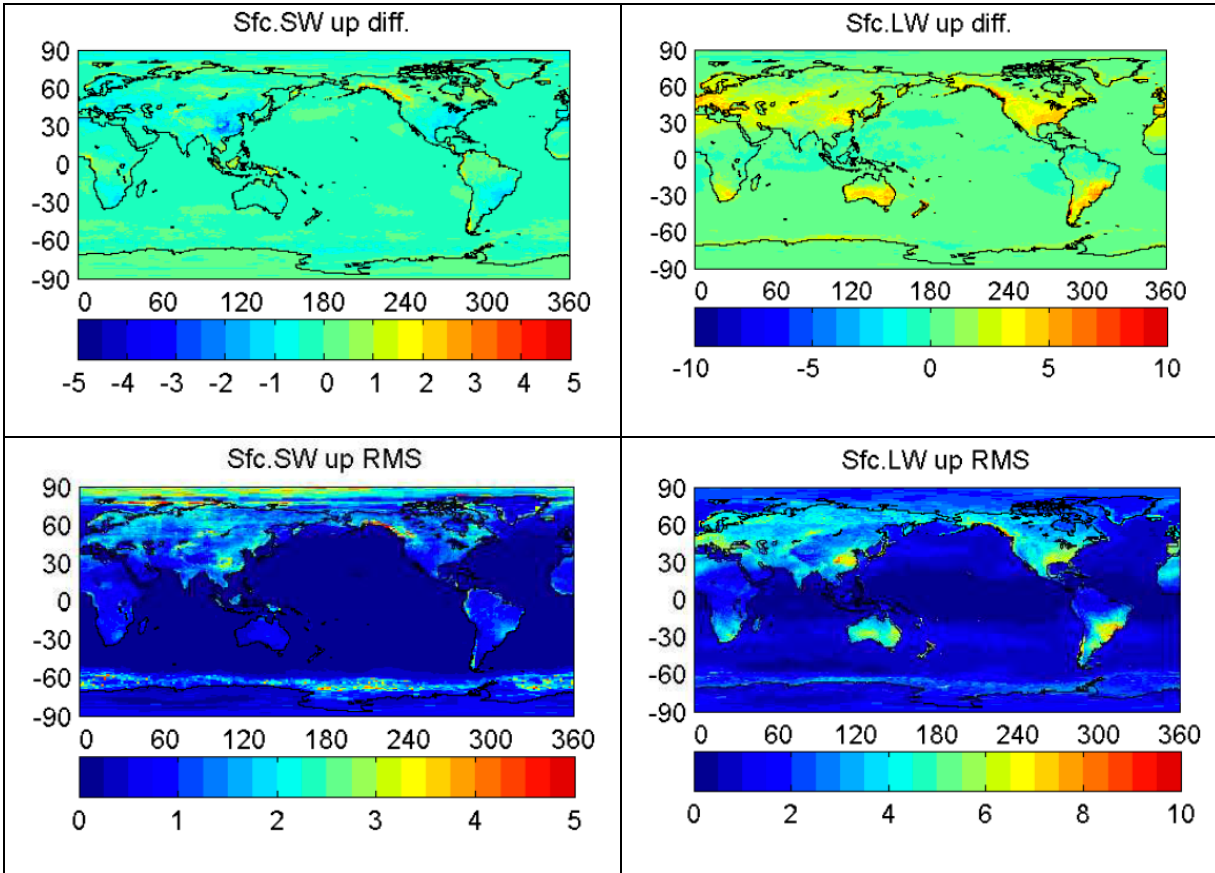
Figure 4-5. (top) Monthly mean difference and (bottom) RMS difference between cloud-removed and clear-sky fraction-weighted (left) surface upward shortwave fluxes and (right) surface upward longwave fluxes in W m^{-2}. The mean difference and RMS difference are computed using 10 years of monthly mean 1°×1° gridded fluxes from March 2000 through February 2010. The mean difference is defined as the clouds-removed minus clear-sky fraction-weighted fluxes.
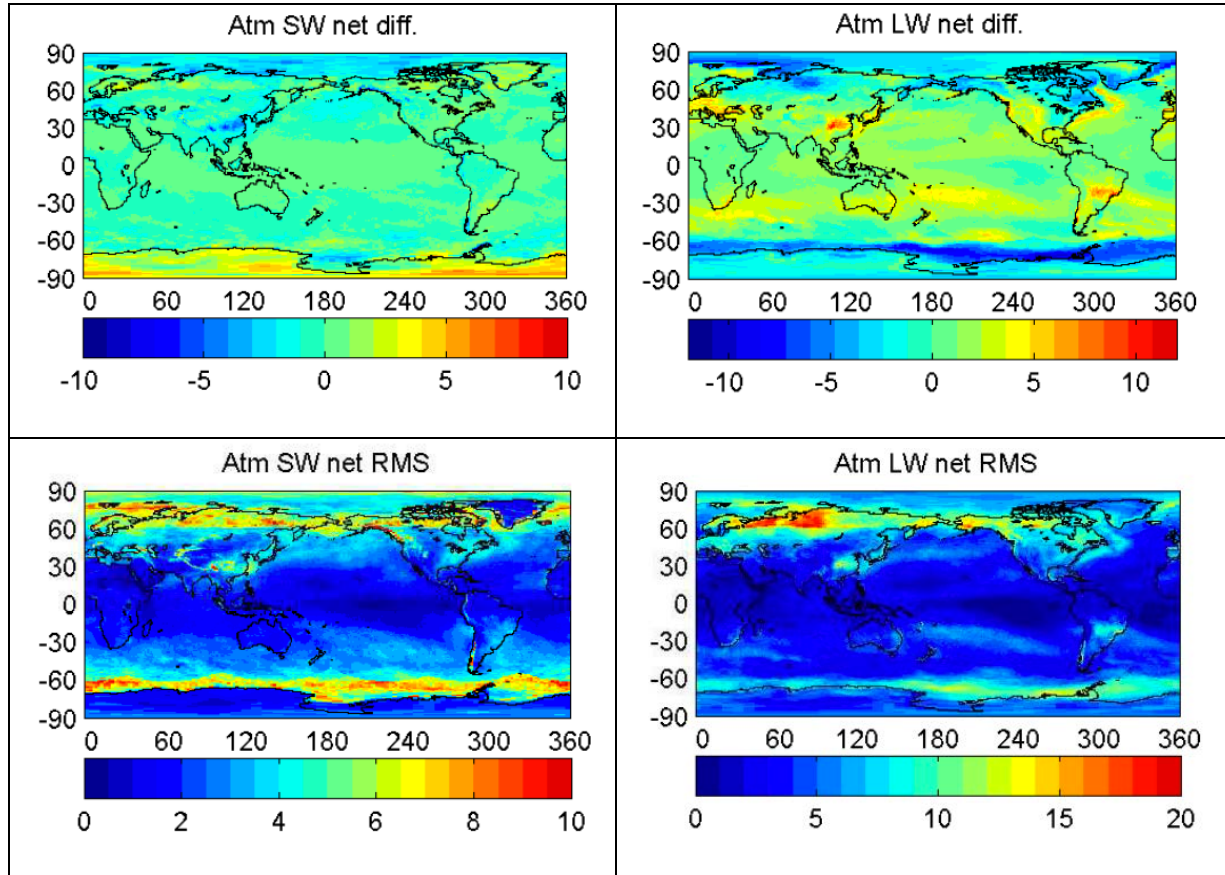
Figure 4-6.   (top) Monthly mean difference and (bottom) RMS difference between cloud-removed and clear-sky fraction-weighted (left) clear-sky atmospheric net shortwave fluxes and (right) clear-sky atmospheric net longwave fluxes in W m^{-2}. The mean difference and RMS difference are computed using 10 years of monthly mean 1°×1° gridded fluxes from March 2000 through February 2010. The mean difference is defined as the clouds-removed minus clear-sky fraction-weighted fluxes. Atmospheric net flux is defined as TOA net minus surface net flux.

4.5   Time Series of Monthly Anomalies

We define deseasonalized anomalies ΔF as

$$\Delta F = F - \overline{F},$$

where F is the surface flux for a given month and $\overline{F}$ is the climatological mean flux for the month. For example, for n years of data, the climatological mean flux computed from n Januaries is subtracted from each January flux to obtain the deseasonalized anomaly for each January. Figure 4-7 shows the time series of global and tropical deseasonalized anomalies of net SW and LW surface fluxes.

Figure 4-7.   Time series of deseasonalized anomalies of global (top) and tropical (bottom) surface net shortwave (blue) and net longwave (red) fluxes.

Because the source of temperature and humidity profiles for flux computations in the Ed3 SYN1deg-Month product was changed from GEOS-4.1 to GEOS-5.2.0 starting in January 2008 a discontinuity in the time series of net surface LW over land was observed in EBAF-Surface Ed2.6r. The CERES team plans to reprocess the entire CERES record with a consistent version of GEOS (GEOS-5.4.1) for the entire suite of CERES data products, including EBAF. In the mean time, EBAF-Surface Ed2.7 uses GEOS-5.4.1 as a reference to remove the discontinuity between GEOS-4.1 and -5.2.0. We first compute the differences in near-surface temperature and humidity between GEOS-5.4.1 and both GEOS-4.1 and GEOS-5.2.0. Based on these differences, the surface fluxes are further adjusted (see Section 4.8 for details). This adjustment significantly reduces a discontinuity over land at the end of 2007 (Figure 4-8 bottom) that is more apparent in Ed2.6r (not shown). Note that the discontinuity that appears in the net LW time series at the end of 2008 over ocean (red line in the top plot of Figure 4-8) is highly unlikely to be due to the GEOS-4.1 to GEOS5.2.0 transition based on two tests to evaluate the adjustment (see Section 4.8 for details). Rather, it is likely related to a strong La Nina event in late 2007 and early 2008.

Some statistical tests to detect discontinuity in a time series (e.g. Menne and Williams 2005) are available. If one computes the mean anomalies from March 2000 through December 2007 and January 2008 through September 2010 from the LW net ocean time series (red line in the top plot of Figure 4-8), the two means are statistically different so that a test given by Hawkins (1977) and a test by Alexanderson (1986) can detect the discontinuity. Even though the two

means are statistically different, the discontinuity is not necessarily caused by artifacts. Because there is no universal rule to detect artifacts in a time series, users who are interested in analyzing trends with this data set are advised to look for physical reasons for a large anomaly, a sudden change, or a large trend. Table 4-4 provides information on the months when inputs were changed. More information is available from
http://ceres.larc.nasa.gov/science_information.php?page=input-data.
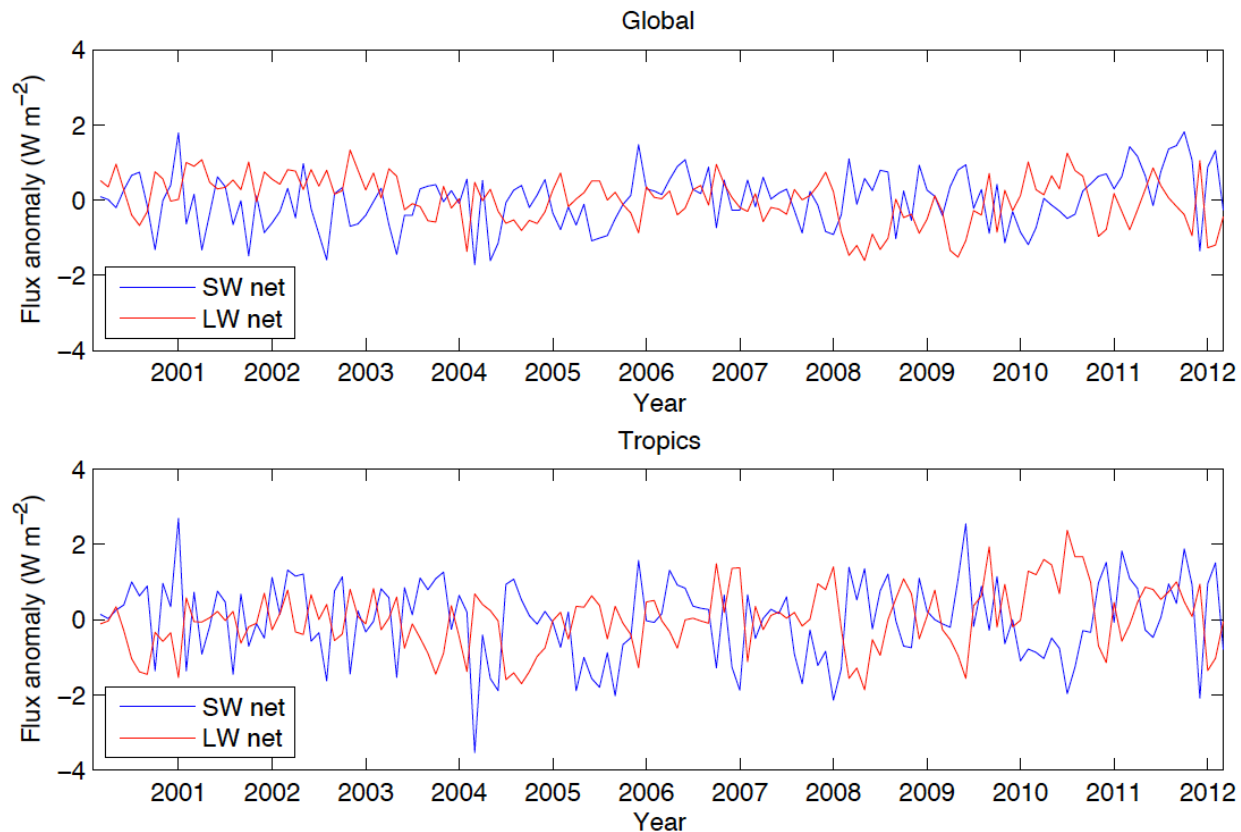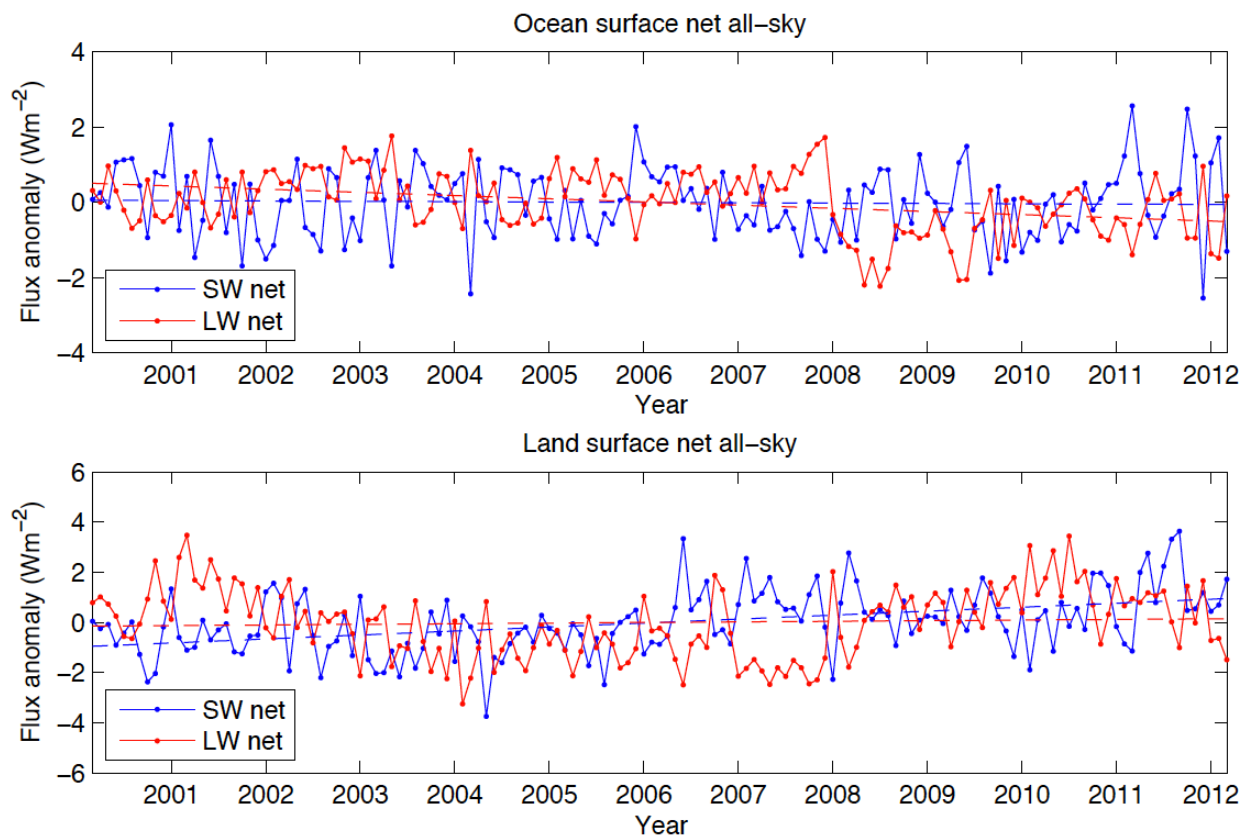

Figure 4-8. Time series of deseasonalized anomalies of global (top) ocean and (bottom) land surface net shortwave (blue line) and net longwave (red line) fluxes. Temperature and relative humidity profiles from GEOS-4 are replaced by GEOS-5 beginning in January 2008.

Table 4-4. Time period of input data sources used for EBAF-Surface production.

Input data source	Starting month	Ending month
GEOS 4.1	March 2000	December 2007
GEOS 5.2.0	January 2008	Current
MODIS Collection 4	March 2000	April 2006
MODIS Collection 5	May 2006	Current

4.6   Comparison of Anomalies with Surface Observations

The deseasonalized anomalies derived from EBAF-Surface are also compared with the deseasonalized anomalies observed at surface sites. Figure 4-9 and Figure 4-10 show that the deseasonalized anomalies from EBAF-Surface agree well with the deseasonalized anomalies observed at both ocean and land stations.
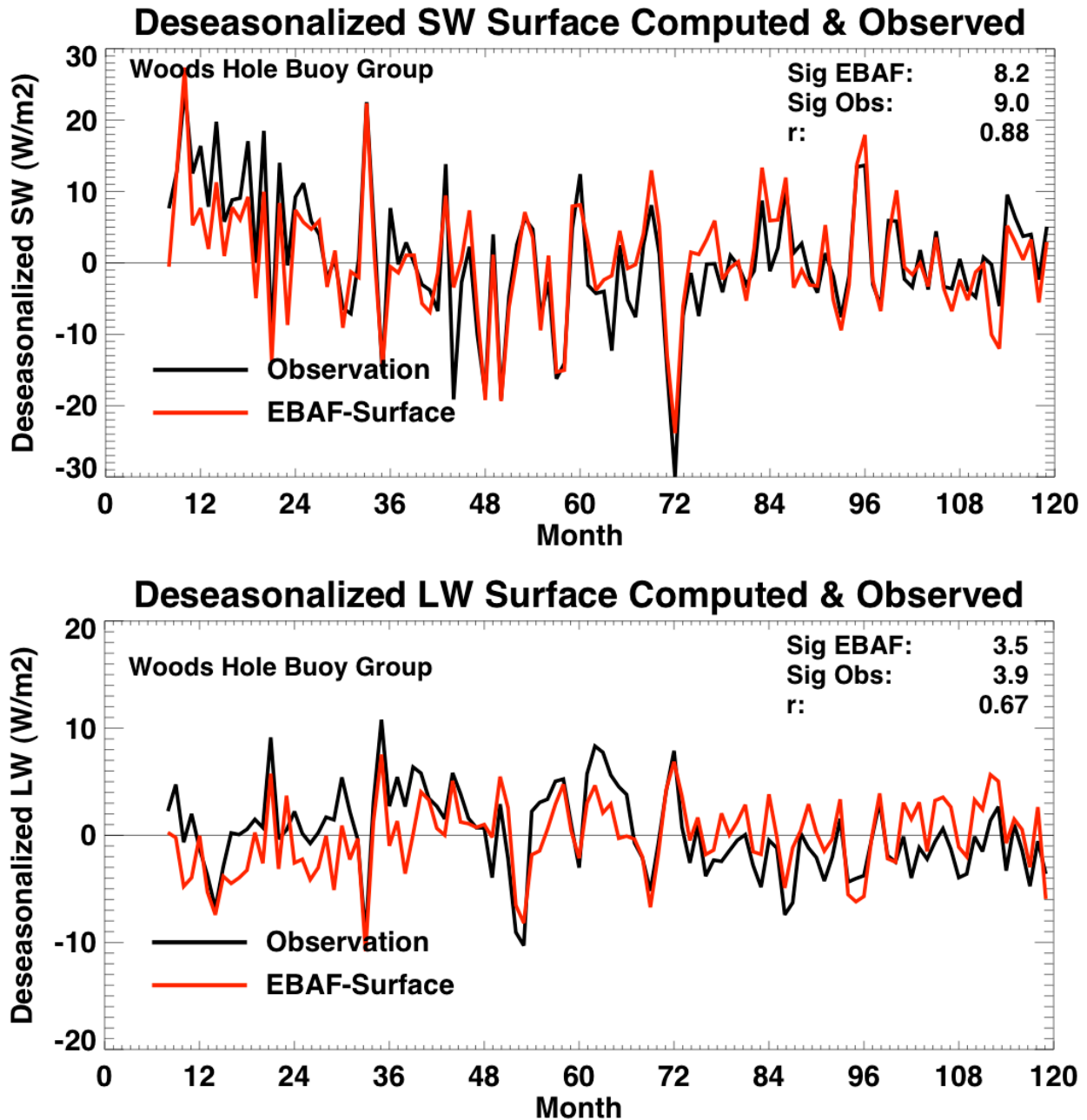
Figure 4-9. Observed deseasonalized anomalies at three ocean buoy sites (black line) for (top) downward SW and (bottom) downward LW. Deseasonalized anomalies derived from EBAF-Surface over grid boxes where ocean surface sites are located are also shown (red line).

Deseasonalized SW Surface Computed & Observed

Level Terrain (Land)

Sig EBAF: 6.7
Sig Obs: 7.3
r: 0.95

Observation
EBAF-Surface

Deseasonalized LW Surface Computed & Observed

Level Terrain (Land)

Sig EBAF: 5.0
Sig Obs: 5.3
r: 0.87

Observation
EBAF-Surface
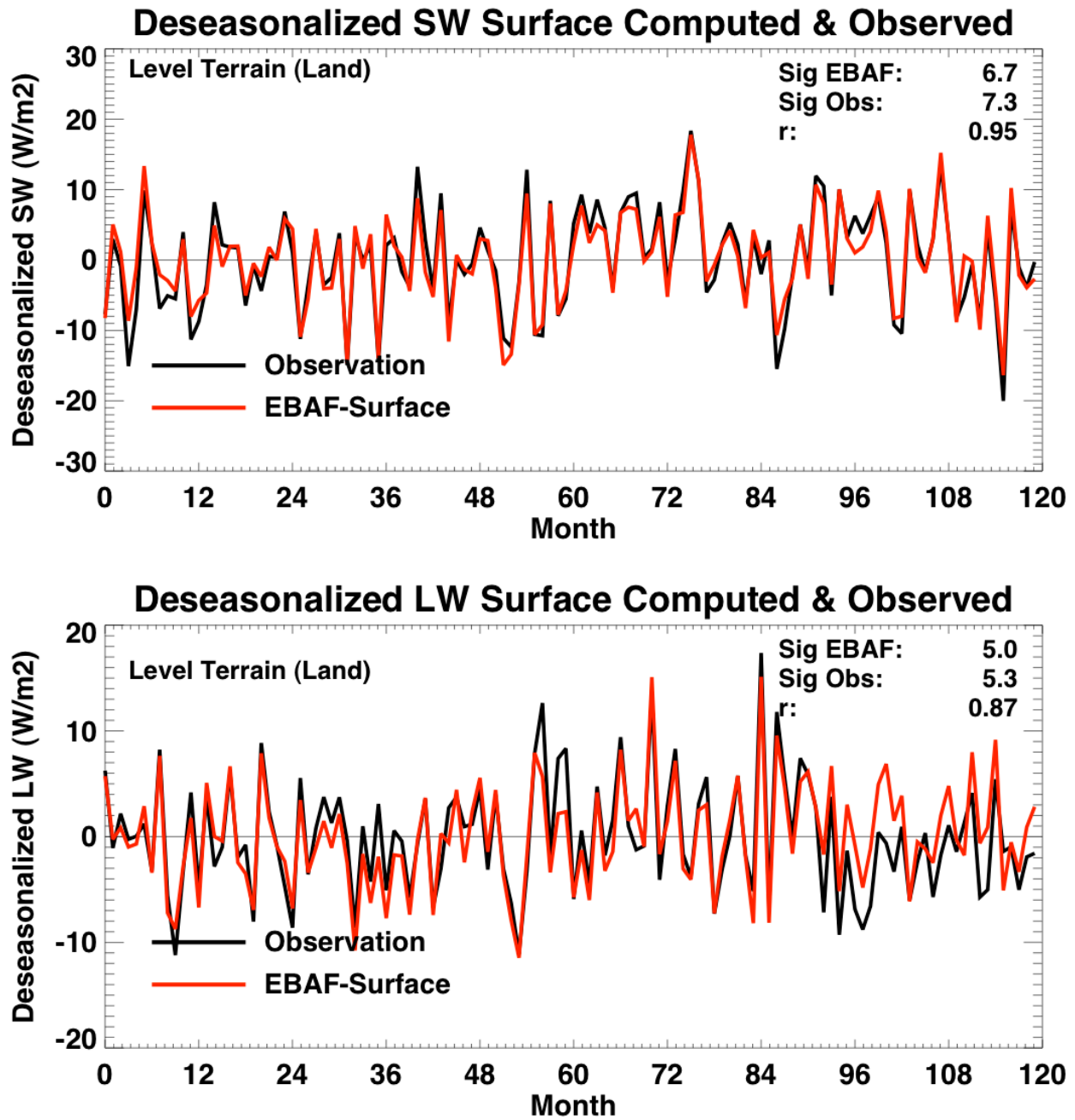
Figure 4-10. Same as Figure 4-9 but for 26 land surface stations.

4.7   Effect of Clear-Sky Sampling on the Anomaly Time Series

In Section 4.4, the clear-sky TOA and surface fluxes computed by removing clouds significantly differ from clear-sky fraction-weighted mean fluxes over some regions. When the global monthly deseasonalized anomaly time series is computed from fluxes calculated by removing clouds and clear-sky fraction-weighted mean fluxes, the two time series are similar (Figure 4-11). This indicates that the spatial sampling difference between the two methods of computing clear-sky fluxes does not affect the global monthly deseasonalized anomaly time series.
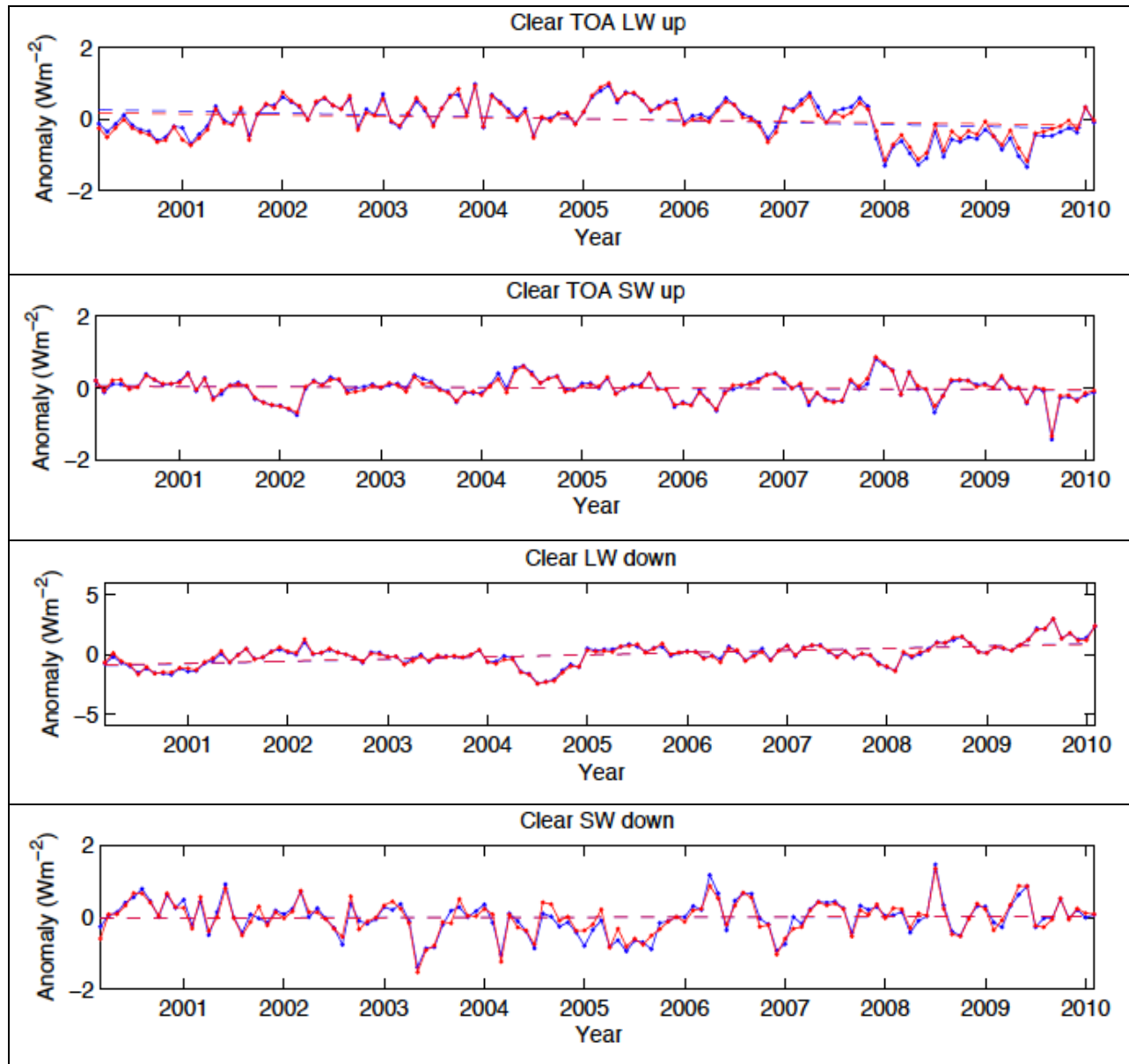
Figure 4-11. Time series of global monthly deseasonalized anomalies computed from clear-sky fraction-weighted average (red line) and from removing clouds (blue line) for (top) TOA upward LW, (second from the top) TOA upward SW, (third from the top) surface downward LW, and (bottom) surface downward SW. Dotted lines are linear regression lines.

17

4.8   Correction of GEOS-4.1 and -5.2 Near-Surface Temperature and Humidity

EBAF Ed2.6r surface LW fluxes are erroneous in 2004 due to a problem with near-surface temperatures and humidities in GEOS-4.1. In addition, GEOS-4.1 temperature and humidity data were used from March 2000-December 2007 and GEOS-5.2 data were used from January 2008 onwards. To mitigate the 2004 problem and the impact of the change in GEOS version, we apply an adjustment based upon GEOS-5.4.1, which does not have erroneous temperature and humidity values in 2004 and which extends over the whole period of EBAF-Surface Ed2.7. Through December 2007, surface LW flux adjustments are derived based upon the difference between surface LW fluxes computed using GEOS-4.1 and GEOS-5.4.1 temperatures and specific humidities for layers with pressure greater than ~900 hPa. Beginning with January 2008, the adjustment uses GEOS-5.2 and GEOS-5.4.1. The adjustments are determined monthly in all 1°×1° regions by numerically derived partial derivatives of surface LW up and downward fluxes with respect to temperature and specific humidity that are multiplied by the difference in values of the two GEOS versions. Figure 4-12 shows the global monthly anomalies of 2 m surface air temperature and specific humidity computed from GEOS-4.1/5.2 and GEOS-5.4.1. Note that relatively large positive specific humidity anomalies occur after 2009 both before and after the correction (Figure 4-12 bottom). Surface observations at nine sites, however, do not show positive specific humidity anomalies at 2 m after 2009. Although the upper tropospheric mean temperature and humidity from GEOS-5.4.1 agree with AIRS-derived temperature and humidity better than those from GEOS-4.1/5.2, the clear-sky TOA LW deseasonalized anomalies computed with GEOS-4.1/5.2 temperature and humidity are correlated with CERES-derived clear-sky TOA LW very well (Figure 4-13). In fact, the correlation coefficeint computed with GEOS-4.1/5.2 is better than that computed with GEOS-5.4.1 (Figure 4-13 bottom). This implies that the GEOS-4.1 problem that happened in 2004 is limited to the lower troposphere.
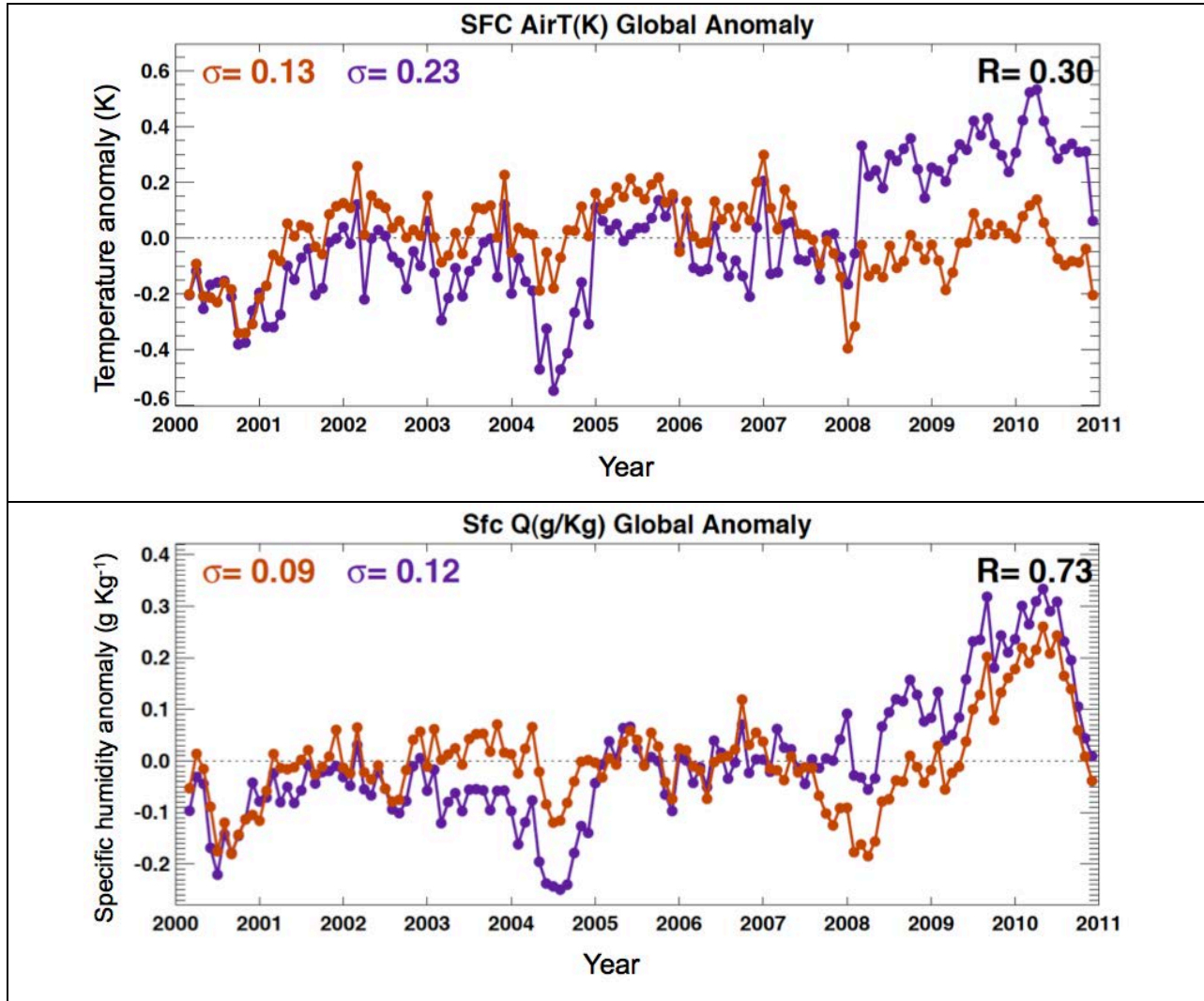
Figure 4-12. Global monthly deseasonalized anomalies of (top) 2 m surface air temperature and (bottom) near-surface specific humidity before (blue line) and after (red line) the adjustment using the GEOS-4.1/5.2 and 5.4.1 difference.
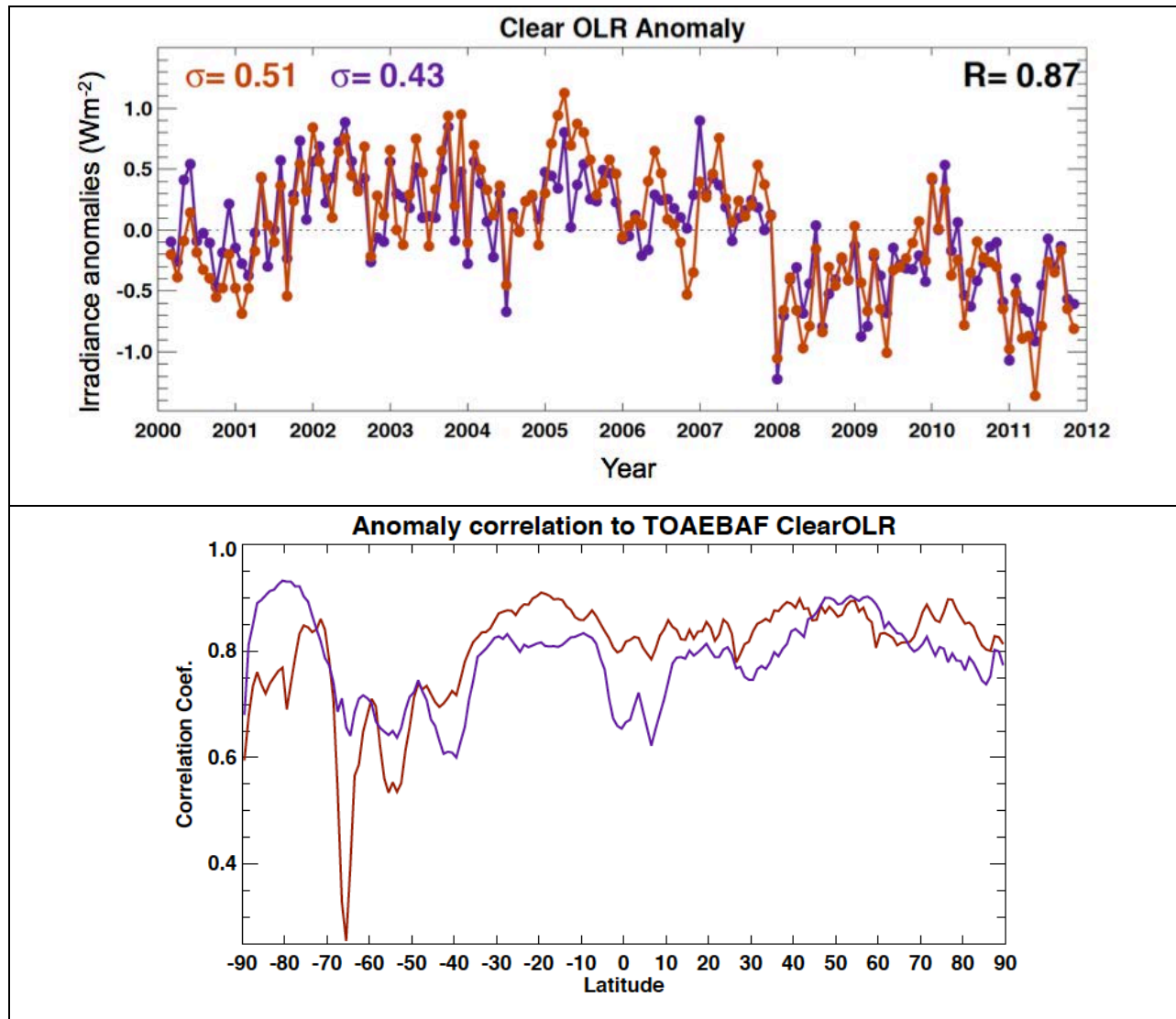
Figure 4-13. (top) Time series of global monthly deseasonalized anomalies of clear-sky TOA LW computed using SYN1deg-Month Ed3A (i.e. before tuning to CERES observation) (red line) and computed using EBAF-TOA Ed2.7 (blue line). (bottom) Correlation coefficient of computed 1° zonal monthly anomalies using GEOS-4.1/5.2 (red line) and using GEOS-5.4.1 (blue line) with CERES-derived EBAF-TOA Ed2.7 clear-sky TOA LW anomalies.

We performed two tests to evaluate the adjustment. In the first test, we use 1°×1° monthly mean temperature and humidity profiles from GEOS-4.1, -5.2, and -5.4.1 to compute the time series of anomalies. The correction is then applied to the clear-sky surface downward LW fluxes computed with GEOS-4.1 as well as GEOS-5.2. This tests whether or not the time series shows any discontinuity at the transition from GEOS-4.1 and GEOS-5.2 in January 2008 and is discussed in Section 4.8.1. For the second test we use one month of SYN1deg produced separately with GEOS-4.1 and GEOS-5.2, apply the correction in each, and examine whether or not the resulting clear-sky surface downward longwave fluxes are consistent with those computed with GEOS-5.4.1 (Section 4.8.2).

4.8.1   Monthly Mean Time Series Test

Figure 4-14 shows the global monthly anomalies computed with GEOS-4.1 and GEOS-5.2 (blue line in the top plot) and with the correction described above (blue line in the bottom plot). The global mean anomalies computed with GEOS-5.4.1 (red lines) are also shown. All anomalies are computed based upon the flux computations with monthly mean 1°×1° gridded atmospheric properties. Our goal is to reduce the ratio of the standard deviations to less than 1.1, that is

$$\frac{\sigma_{corr}}{\sigma_{541}} < 1.1,$$

where σ_{corr} is the standard deviation of the clear-sky surface downward longwave flux deseasonalized anomaly computed with GEOS-4.1/5.2 with the correction and σ_{541} is the standard deviation of the deseasonalized anomalies computed with GEOS-5.4.1. This goal is equivalent to increasing the trend uncertainty by no more than 10% (Wielicki et al. 2013). Monthly anomalies separated by land and ocean are shown in Figure 4-15. Table 4-5 summarizes the standard deviations computed using global deseasonalized anomalies and deseasonalized anomalies over land and ocean and shows that our goal is achieved globally and over ocean and land.
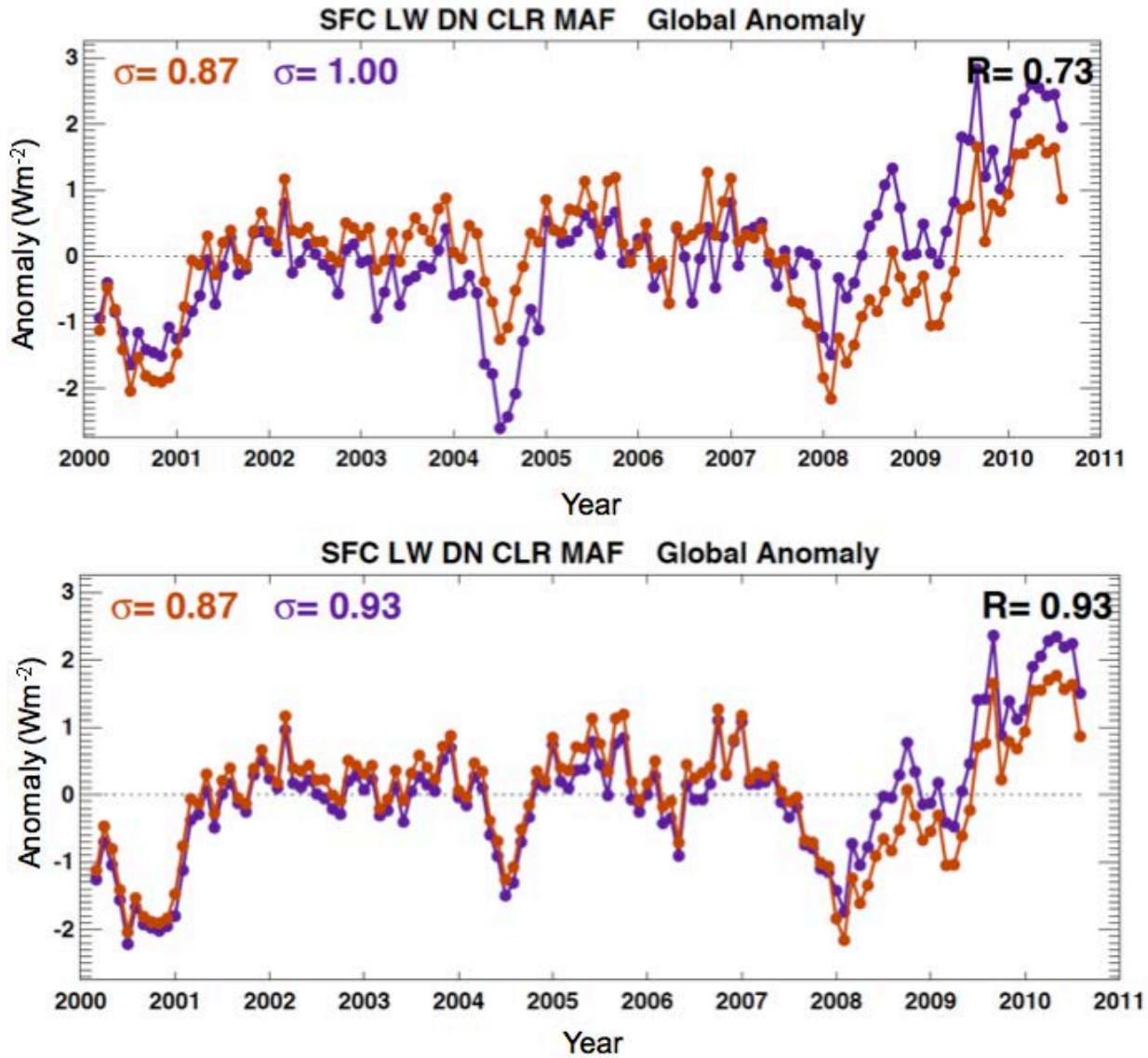
Figure 4-14. Global monthly mean deseasonalized anomalies of clear-sky surface downward longwave flux (top) before the adjustment and (bottom) after the adjustment (blue line in each plot). The computations use GEOS-4.1 from March 2000 and switch to GEOS-5.2 in January 2008. These anomalies are computed with 1°×1° monthly mean inputs to simulate the correction discussed in Section 4.8. The red lines in both plots are the same and indicate the anomalies computed with GEOS-5.4.1 for the entire period.

SFC LW DN CLR MAF   Ocean Anomaly

SFC LW DN CLR MAF   Land Anomaly
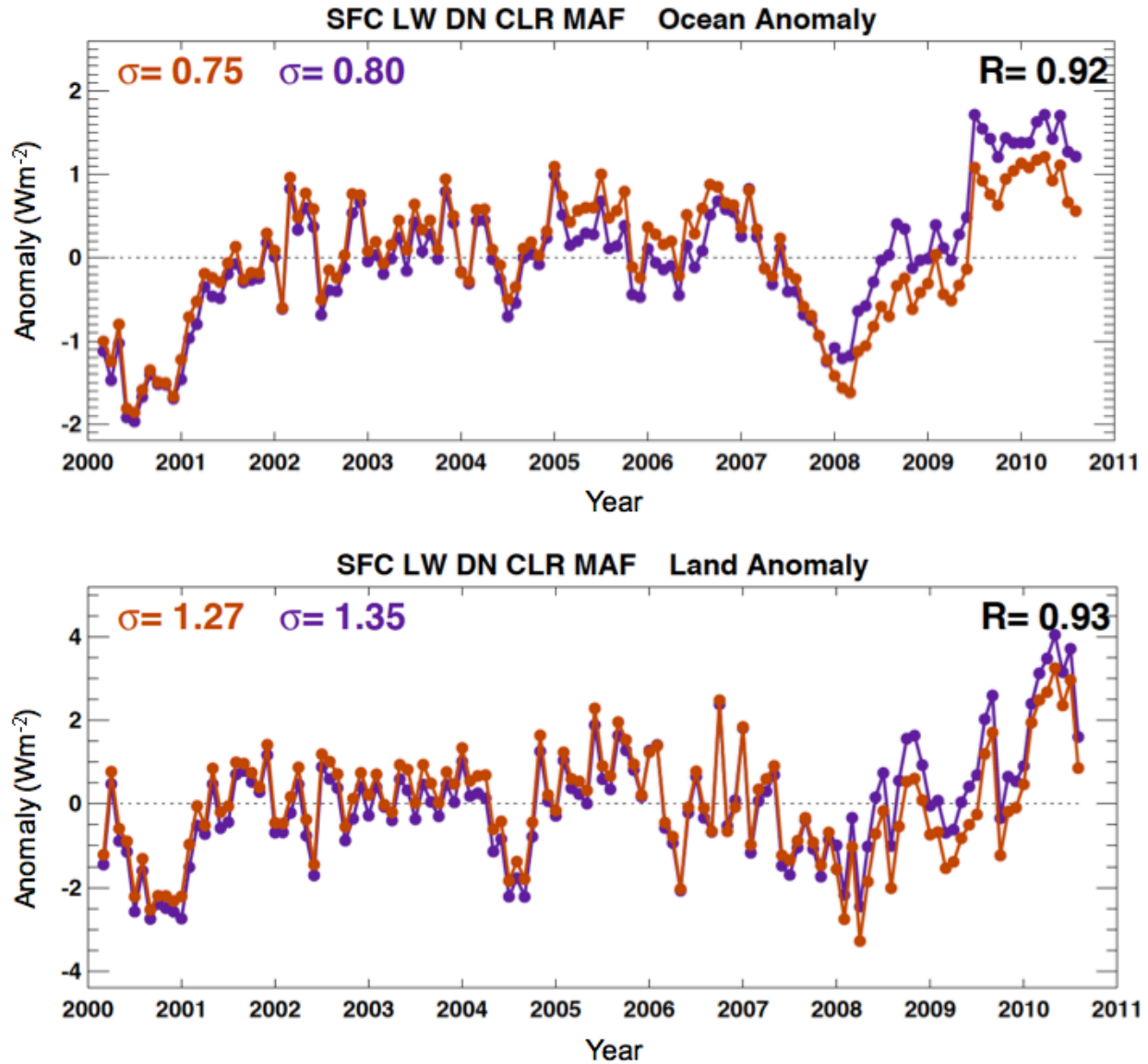
Figure 4-15. Global monthly mean deseasonalized anomalies of clear-sky surface downward longwave flux over (top) ocean and (bottom) land after the adjustment (blue line in each plot). The computations use GEOS-4.1 from March 2000 and switch to GEOS-5.2 in January 2008. These anomalies are computed with $1° \times 1°$ monthly mean inputs to simulate the correction discussed in Section 4.8. The red lines in both plots indicate the anomalies computed with GEOS-5.4.1 for the entire period.

Table 4-5. Standard deviation of clear-sky surface downward longwave flux anomalies.

	σ_{corr} (Wm^{-2})	σ_{541} (Wm^{-2})	$\sigma_{corr}/\sigma_{541}$
Global	0.93	0.87	1.07
Ocean	0.80	0.75	1.07
Land	1.35	1.27	1.06

4.8.2   One Month of Clear-Sky Surface Downward Longwave Irradiance Test Using SYN1deg-Month

Figure 4-16 shows the difference between the monthly gridded mean clear-sky surface downward longwave flux produced with GEOS-4.1 or GEOS-5.2 and GEOS-5.4.1 for December 2007. The correction is applied to the longwave irradiance produced using GEOS-4.1 or -5.2. If the correction is perfect, the difference is zero, because the goal is to make the clear-sky surface fluxes as if they were produced using GEOS-5.4.1. The global mean clear-sky surface downward longwave irradiance using either GEOS-4.1 and GEOS-5.2 (after the correction is applied) differs by -0.3 W m^{-2} from that computed using GEOS-5.4.1. To be consistent with the first test, our goal of the second test is

$$\left[\frac{\sigma_{541}^2 + \Delta F_x^2}{\sigma_{541}^2} \right]^{1/2} < 1.1,$$

where $\Delta F_x = F_x - F_{541}$, F_x is the global mean clear-sky surface downward longwave flux computed using either GEOS-4.1 or -5.2, and F_{541} is the global mean clear-sky surface downward longwave flux computed using GEOS-5.4.1. Because the standard deviation of the global monthly anomaly σ_{541} is 0.87 W m^{-2}, the differences ΔF_4 and ΔF_{52} have to be less than 0.40 to meet our criteria, i.e. $\left| \Delta F_x \right| < 0.40$. The result shown in Figure 4-16 meets this goal.
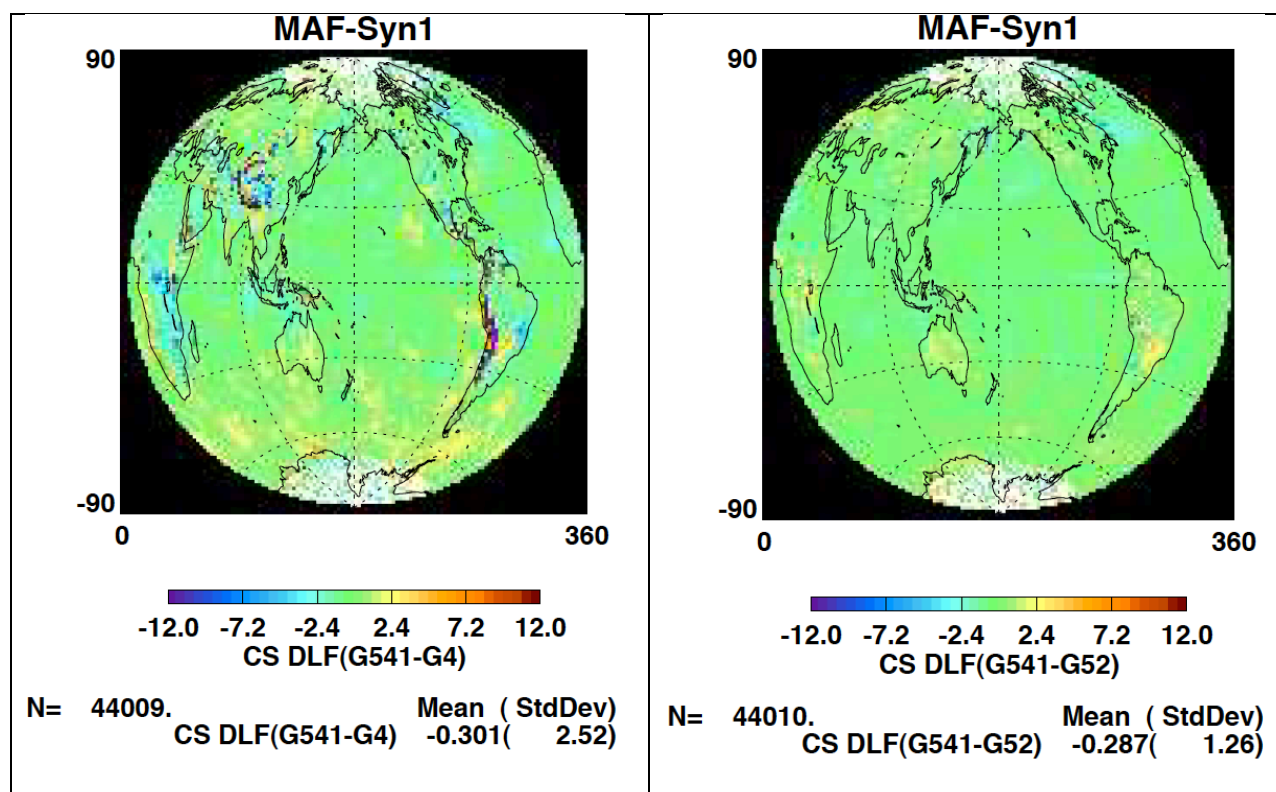
Figure 4-16. (left) Difference of the 1°×1° gridded monthly mean clear-sky surface downward longwave irradiance produced using GEOS-5.4.1 and GEOS-4.1. The correction described in Section 4.8 is applied to the irradiance computed with GEOS-4.1. (right) Same as the left plot but using GEOS-5.2.

4.9   Trend in Clear-Sky Surface Downward Shortwave Flux

When the trend in clear-sky downward shortwave surface flux is computed from EBAF-Surface, some regions over land show a large trend (Figure 4-17). This is mostly caused by changing the aerosol source from MODIS Collection 4 to Collection 5 at the end of April 2006. Over land, the Collection 4 aerosol optical thickness generally exceeds that in Collection 5. This results in a positive trend in the clear-sky downward shortwave flux and is evident over Eurasia and eastern North America. However, some regions show a negative trend. This is because the aerosol data come from two sources: MODIS and Model of Atmospheric Transport and Chemistry (MATCH, Collins et al. 2001). MATCH is an aerosol transport model that assimilates MODIS aerosol optical thickness. When the MODIS aerosol optical thickness passes a series of quality tests, the MODIS aerosol optical thickness is used for flux computations. If the MODIS aerosol optical thickness is missing or fails the quality tests, the aerosol optical thickness from MATCH is used. In some regions, the Collection 4 aerosol optical thickness at 660 nm is larger than that at 470 nm. When this happens, the MODIS Collection 4 aerosol optical thickness does not pass our quality test, and MATCH-derived aerosol optical thickness is used for these regions. This spectral aerosol optical thickness problem happens much less in MODIS Collection 5. When the MATCH aerosol optical thickness is significantly less than the MODIS Collection 4 aerosol

25

optical thickness and is also less than the Collection 5 aerosol optical thickness for a later time over the same region, a positive trend of aerosol optical thickness is introduced along with a corresponding negative trend of clear-sky downward shortwave irradiance. An example of this negative trend can be seen over western North America (Figure 4-17).

The top plot in Figure 4-18 also shows that a large difference exists between MODIS-derived (black line) and multi-filter rotating shadowband radiometer (MFRSR)-derived (blue line) aerosol optical thickness over Desert Rock, Nevada. We have not investigated the difference of MODIS-derived and ground-based aerosol optical thickness for other sites. Deseasonalized anomalies of computed (black line) clear-sky downward shortwave fluxes over the Desert Rock, Nevada, US surface site show a discontinuity while observed flux anomalies (red line) do not show such discontinuity (Figure 4-18 bottom). Users interested in the aerosol direct radiative effect at the surface over land need to use caution due to these issues. The artificial trend problem causd by the two versions of MODIS aerosol products will be eliminated in a future reprocessing of CERES data products (Edition 4) that will use a consistent version of MODIS aerosols.
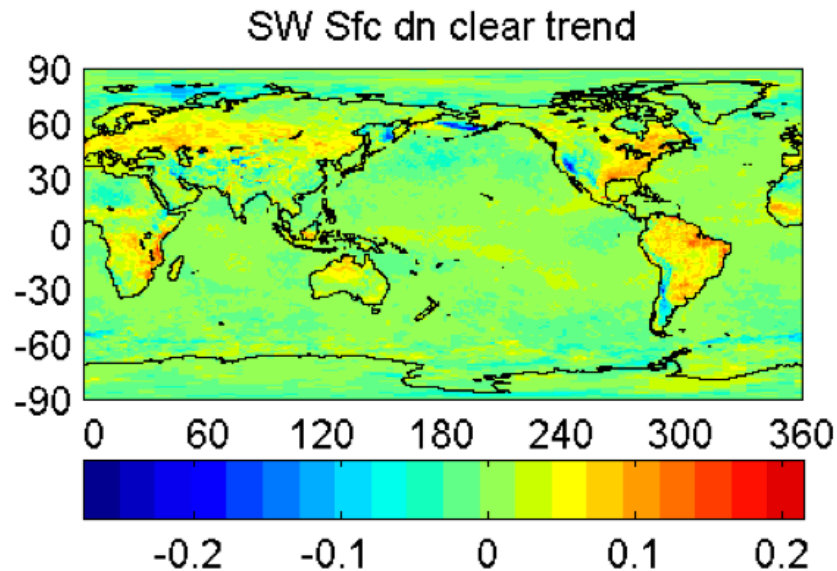
Figure 4-17. Slope of linear regression applied to 1°×1° monthly clear-sky surface downward shortwave irradiances in W m^{-2} month^{-1} computed with 133 months of data. The large positive slopes over North America and Eurasia are caused by changing the input source of aerosol optical thickness from MODIS Collection 4 to Collection 5.

AOT @550nm

Deseasonsalized SW Surface Irradiance Down
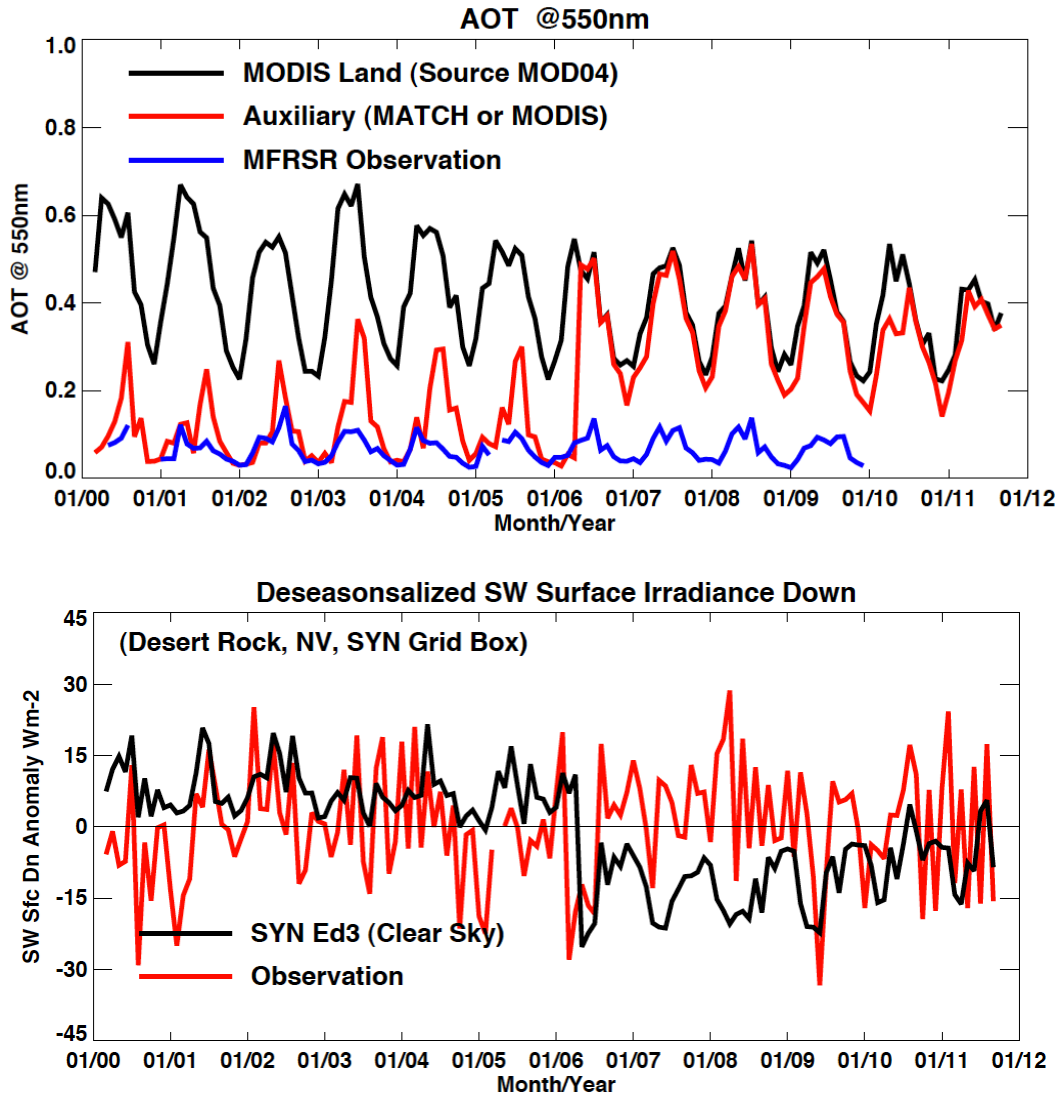
Figure 4-18.   (top) Time series of aerosol optical thickness (red line) for surface flux computations from the SYN1deg-Month 1°×1° grid box over the Desert Rock, Nevada, US surface site. The SYN1deg-Month product is used as input to the EBAF-Surface product. Black and blue lines are MODIS-derived and MFRSR-derived aerosol optical thickness. (bottom) Deseasonalized anomalies of computed (black) and observed (red) downward shortwave fluxes over the Desert Rock, Nevada, US surface site.

5.0   References

The full version of CERES EBAF-Surface_Ed2.7 is available from the following ordering site:

http://ceres.larc.nasa.gov/order_data.php

Alexanderson, H., 1986: A homogeneity test applied to precipitation data, *J. Climatol*., 6, 661-675.

Barker, H. W., 1996: A parameterization for computing grid-averaged solar fluxes for inhomogeneous marine boundary layer clouds. Part I: Methodology and homogeneous biases. *J. Atmos. Sci.*, 53, 2289-2303.

Bloom, S. A., and Coauthors, 2005: Documentation and validation of the Goddard Earth Observing System (GEOS) Data Assimilation System Version-4. NASA Tech. Rep. NASA/TM-2005-104606, Vol. 26, 187 pp.

Bourlès, B., and Coauthors, 2008: The PIRATA Program: History, accomplishments, and future directions. *Bull. Amer. Meteor. Soc*., 89, 1111–1125.

Cess, R. D. and G. L. Potter, 1987: Exploratory studies of cloud radiative forcing with a general circulation model. *Tellus*, 39A, 460-473.

Collins, W. D., P. J. Rasch, B. E. Eaton, B. V. Khattatov, J.-F. Lamarque, and C. S. Zender, 2001: Simulating aerosols using a chemical transport model with assimilation of satellite aerosol retrievals: Methodology for INDOEX. *J. Geophys. Res.*, 106, 7313–7336.

Doelling, D. R., N. G. Loeb, D. F. Keyes, M. L. Nordeen, D. Morstad, B. A. Wielicki, D. F. Young, and M. Sun, 2013: Geostationary enhanced temporal interpolation for CERES flux products, *J. Atmos. Oceanic Technol*., in press.

Fu, Q., K. Liou, M. Cribb, T. Charlock, and A Grossman, 1997: On multiple scattering in thermal infrared radiative transfer. *J. Atmos. Sci*., 54, 2799-2812.

Jin, Z., T. P. Charlock, W. L. Smith, Jr., and K. Rutledge, 2004: A look-up table for ocean surface albedo. *Geophys. Res. Lett*., 31, L22301.

Hawkins, D. M., 1977: Testing a sequence of observations for a shift in location, *J. Am. Stat. Assoc.*, 72, 180-186.

Kato, S. and N. G. Loeb, 2003: Twilight irradiance reflected by the Earth estimated from Clouds and the Earth's Radiant Energy System (CERES) measurements. *J. Climate*, 16, 2646-2650.

Kato, S., F. G. Rose, and T. P. Charlock, 2005: Computation of domain-averaged irradiance using satellite derived cloud properties. *J. Atmos. Oceanic Technol*., 22, 146-164.

Kato, S., and Coauthors, 2011: Improvements of top-of-atmosphere and surface irradiance computations with CALIPSO-, CloudSat-, and MODIS-derived cloud and aerosol properties. *J. Geophys. Res*., 116, D19209, doi:10.1029/2011JD016050.

Kato, S., N. G. Loeb, D. A. Rutan, F. G. Rose, S. Sun-Mack, W. F. Miller, and Y. Chen, 2012: Uncertainty estimate of surface irradiances computed with MODIS-, CALIPSO-, and CloudSat-derived cloud and aerosol properties. *Surv. Geophys.*, doi:10.1007/s10712-012-9179-x.

Kato, S., N. G. Loeb, F. G. Rose, D. R. Doelling, D. A. Rutan, T. E. Caldwell, L. Yu, and R. A. Weller, 2013: Surface irradiances consistent with CERES-derived top-of-atmosphere shortwave and longwave irradiances, *J. Climate*, 26, 2719-2740, doi:10.1175/JCLI-D-12-00436.1.

Loeb, N. G., B. A. Wielicki, D. R. Doelling, G. L. Smith, D. F. Keyes, S. Kato, N. Manalo-Smith, and T. Wong, 2009: Toward optimal closure of the Earth's top-of-atmosphere radiation budget. *J. Climate*, 22, 748-766.

Loeb, N. G., J. M. Lyman, G. C. Johnson, R. P. Allan, D. R. Doelling, T. Wong, B. J. Soden, and G. L. Stephens, 2012: Observed changes in top-of-the-atmosphere radiation and upper-ocean heating consistent within uncertainty. *Nat. Geosci.*, 5, 110-113. doi:10.1038/NGEO1375.

McPhaden, M. J., and Coauthors, 1998: The Tropical Ocean–Global Atmosphere observing system: A decade of progress. *J. Geophys. Res.*, 103, 14 169–14 240.

McPhaden, M. J., and Coauthors, 2009: RAMA: The Research Moored Array for African–Asian–Australian Monsoon Analysis and Prediction. *Bull. Amer. Meteor. Soc.*, 90, 459–480.

Menne, M. J., and C. N. Williams, 2005: Detection of undocumented changepoints using multiple test statistics and composite reference series, *J. Climate*, 18, 4271-4286.

Minnis, P., W. L. Smith, Jr., D. P. Garber, J. K. Ayers, and D. R. Doelling, 1995: Cloud properties derived from GOES-7 for Spring 1994 ARM intensive observing period using Version 1.0.0 of ARM Satellite Data Analysis Program. NASA Ref. Pub. NASA-RP-1366, 62 pp.

Minnis, P. and Coauthors, 2011: CERES Edition-2 cloud property retrievals using TRMM VIRS and Terra and Aqua MODIS data, Part I: Algorithms. *IEEE Trans. Geosci. Remote Sens.* 49, doi: 10.1109/TGRS.2011.2144601.

Oreopoulos, L. and H. W. Barker, 1999: Accounting for subgrid-scale cloud variability in a multi-layer 1D solar radiative transfer algorithm. *Quart. J. Roy. Meteor. Soc.* 125, 301-330.

Rienecker, M. M. and Coauthors, 2008: The GOES-5 Data Assimilation System-Documentation of Versions 5.0.1, 5.1.0, and 5.2.0. NASA Tech. Rep. NASA/TM-2009-104606, Vol. 27, 118 pp.

Rose, F., D. A. Rutan, T. P. Charlock, G. L. Smith, and S. Kato, 2013: An algorithm for the constraining of radiative transfer calculations to CERES observed broadband top of atmosphere irradiance, *J. Atmos. Oceanic Technol.*, in press.

Rutan, D., F. Rose, M. Roman, N. Manalo-Smith, C. Schaaf, and T. Charlock, 2009: Development and assessment of broadband surface albedo from Clouds and the Earth's

Radiant Energy System clouds and radiation swath data product. *J. Geophys. Res*., 114, D08125, doi:10.1029/2008JD010669.

Sohn, B. J., T. Nakajima, M. Satoh, and H.-S. Jang, 2010: Impact of different definitions of clear-sky flux on the determination of longwave cloud radiative forcing: NICAM simulation results. *Atmos. Chem. Phys*., 10, 11641-11646, doi:105194/acp-10-11641-2010.

Toon, O. B., C. P. Mckay, T. P. Ackerman and K. Santhanam, 1989: Rapid calculation of radiative heating rates and photodissociation rates in inhomogeneous multiple scattering atmospheres. *J. Geophys. Res*., 94, 16 287–16 301.

Wielicki, B. A., and Coauthors, 2013: Achieving climate change absolute accuracy in orbit. *Bull. Amer. Met. Soc.,* in press.

Yang, S.-K., S. Zhou, and A. J. Miller, 2000: SMOBA: A 3-D daily ozone analysis using SBUV/2 and TOVS measurements.
http://www.cpc.ncep.noaa.gov/products/stratosphere/SMOBA/smoba_doc.shtml.

6.0   Attribution

When referring to the CERES EBAF-Surface product, please include the data set version and the data product as "CERES EBAF-Surface_Ed2.7."

The CERES Team has made considerable efforts to remove major errors and to verify the quality and accuracy of this data. Please provide a reference to the following paper when you publish scientific results with the

CERES EBAF-Surface_Ed2.7

Kato, S., N. G. Loeb, F. G. Rose, D. R. Doelling, D. A. Rutan, T. E. Caldwell, L. Yu, and R. A. Weller, 2013: Surface irradiances consistent with CERES-derived top-of-atmosphere shortwave and longwave irradiances. *J. Climate*, 26, 2719-2740, doi:10.1175/JCLI-D-12-00436.1.

When CERES data that are obtained via the CERES web site are used in a publication, we request the following acknowledgment be included: "These data were obtained from the NASA Langley Research Center CERES ordering tool at (http://ceres.larc.nasa.gov/)."

7.0   Feedback and Questions

For questions or comments on the CERES EBAF-Surface Data Quality Summary, please contact Dr. Seiji Kato, seiji.kato@nasa.gov. For questions about the CERES subsetting/visualization/ordering tool at http://ceres.larc.nasa.gov/order_data.php, please click on the "Feedback" link on the left-hand banner.